STRUCTURAL BIOLOGY COMMUNICATIONS

ISSN 2053-230X

Crystal structure of *Halobacterium salinarum* halorhodopsin with a partially depopulated primary chloride-binding site

Madeleine Schreiner,[a] Ramona Schlesinger,[b] Joachim Heberle[c] and Hartmut H. Niemann[a]*

[a]Department of Chemistry, Bielefeld University, Universitätsstrasse 25, 33615 Bielefeld, Germany, [b]Genetic Biophysics, Freie Universität Berlin, Arnimallee 14, 14195 Berlin, Germany, and [c]Experimental Molecular Biophysics, Freie Universität Berlin, Arnimallee 14, 14195 Berlin, Germany. *Correspondence e-mail: hartmut.niemann@uni-bielefeld.de

Received 28 April 2016
Accepted 8 August 2016

Edited by M. S. Weiss, Helmholtz-Zentrum Berlin für Materialien und Energie, Germany

Keywords: halorhodopsin; *Halobacterium salinarum*; archaeal rhodopsin; retinal protein; light-driven ion pump; post-crystallization treatment; reaction intermediate.

PDB reference: halorhodopsin in a new rhombohedral crystal form, 5g36

Supporting information: this article has supporting information at journals.iucr.org/f

The transmembrane pump halorhodopsin in halophilic archaea translocates chloride ions from the extracellular to the cytoplasmic side upon illumination. In the ground state a tightly bound chloride ion occupies the primary chloride-binding site (CBS I) close to the protonated Schiff base that links the retinal chromophore to the protein. The light-triggered *trans–cis* isomerization of retinal causes structural changes in the protein associated with movement of the chloride ion. In reverse, chemical depletion of CBS I in *Natronomonas pharaonis* halorhodopsin (*Np*HR) through deprotonation of the Schiff base results in conformational changes of the protein: a state thought to mimic late stages of the photocycle. Here, crystals of *Halobacterium salinarum* halorhodopsin (*Hs*HR) were soaked at high pH to provoke deprotonation of the Schiff base and loss of chloride. The crystals changed colour from purple to yellow and the occupancy of CBS I was reduced from 1 to about 0.5. In contrast to *Np*HR, this chloride depletion did not cause substantial conformational changes in the protein. Nevertheless, two observations indicate that chloride depletion could eventually result in structural changes similar to those found in *Np*HR. Firstly, the partially chloride-depleted form of *Hs*HR has increased normalized *B* factors in the region of helix C that is close to CBS I and changes its conformation in *Np*HR. Secondly, prolonged soaking of *Hs*HR crystals at high pH resulted in loss of diffraction. In conclusion, the conformation of the chloride-free protein may not be compatible with this crystal form of *Hs*HR despite a packing arrangement that hardly restrains helices E and F that presumably move during ion transport.

1. Introduction

Halophilic archaea thrive in highly saturated brines. Residing in such extreme environments poses a notable challenge to the metabolism of these unicellular organisms (Falb *et al.*, 2008; Reed *et al.*, 2013). In order to maintain the osmotic balance, chloride ions have to be constantly transported into the cytoplasm. This task is facilitated by a family of light-sensitive, membrane-localized proteins known as halorhodopsins (HRs), the distribution of which is confined to halophilic archaea (Schobert & Lanyi, 1982; Lanyi, 1990).

HR is a seven-pass transmembrane protein (helices A–G) with an extracellular N-terminus (Kolbe *et al.*, 2000). The retinal chromophore is covalently attached to a lysine in helix G *via* a Schiff base. The primary chloride-binding site (CBS I) is located on the extracellular side next to the protonated Schiff base (PSB). In addition, there is a second, peripheral extracellular chloride-binding site (CBS II). On activation by yellow/orange light, HR traverses a reversible photocycle that consists of several distinct intermediate states with distinct

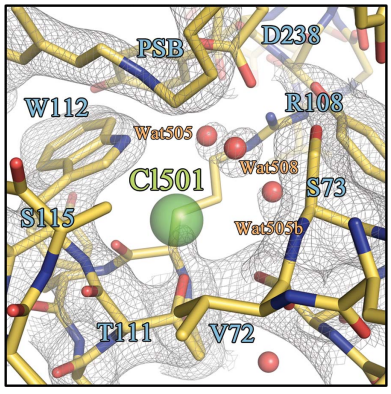

spectroscopic properties. In the course of this process HR actively transports a single halide ion, preferably chloride, from the environmental medium into the cytoplasm. The transport process is triggered by the light-induced all-*trans* to 13-*cis* isomerization of retinal.

To date, the halorhodopsins from *Halobacterium salinarum* (*Hs*HR) and *Natronomonas pharaonis* (*Np*HR) are the most extensively studied members of the halorhodopsin family. Since the discovery of *Hs*HR in the 1980s (Luisi *et al.*, 1980; Mukohata & Kaji, 1981), several attempts have been made to elucidate the ion transport at the molecular level using spectroscopic methods (Ames *et al.*, 1992; Váró, Zimányi *et al.*, 1995) and by crystallography. The latter revealed structures of the ground state and the L1-intermediate at high resolution (Kolbe *et al.*, 2000; Gmelin *et al.*, 2007). Despite these remarkable accomplishments, the molecular mechanism facilitating ion transport has long remained elusive. Recent studies of *Np*HR provided valuable information on the progression of structural changes and the route of the extracellular ion-transport pathway (Kanada *et al.*, 2011; Kouyama *et al.*, 2015). However, although both *Hs*HR and *Np*HR belong to the halorhodopsin family, they are only distantly related (the *Np*HR sequence is 60% identical to *Hs*HR and is 16 amino acids longer) and thus differ significantly in ion specificity and photocycle kinetics. Those differences are most prominent in the late stages of the photocycle. Hence, information gained on *Np*HR can be transferred to *Hs*HR only to a limited extent. In *Np*HR, ion release into the cytoplasm has been shown to be associated with the O-intermediate (Guijarro *et al.*, 2006; Kanada *et al.*, 2011; Kouyama *et al.*, 2015), the decay of which is also the rate-determining step within the *Np*HR photocycle (Váró, Brown *et al.*, 1995; Váró, Needleman *et al.*, 1995), while in *Hs*HR it is the decay of the L2-intermediate (Spencer & Dewey, 1990; Váró, Zimányi *et al.*, 1995). Furthermore, to date, most probably owing to kinetic reasons, a red-shifted O-like state has not been detected spectroscopically in *Hs*HR under native conditions (Zimányi & Lanyi, 1989; Váró, Zimányi *et al.*, 1995; Rüdiger & Oesterhelt, 1997) and thus the existence of this intermediate is still under extensive discussion. Although there is still disagreement on the assignment and occurrence of late intermediates, an anion-free form, like the *Np*HR O-state, has to exist to yield a closed photocycle.

In order to further elucidate the ion-transport mechanism of *Hs*HR at the molecular level, we attempted to trap late-photocycle intermediates in *Hs*HR crystals and determine their structure. Apart from photoactivation of HR, intermediates resembling late stages of the photocycle after ion release to the cytoplasm has occurred can also be generated by chemical modification of the protein (Lanyi & Schobert, 1983; Hazemoto *et al.*, 1984; Hegemann *et al.*, 1985; Kanada *et al.*, 2011). Owing to a relatively high halide-ion affinity, ion release from CBS I near the PSB does not occur easily (Falke *et al.*, 1984; Steiner *et al.*, 1984; Váró, Zimányi *et al.*, 1995). Yet, the ion affinity can be significantly reduced upon deprotonation of the PSB (Schobert *et al.*, 1986; Kanada *et al.*, 2011). This process leads to the formation of a yellow form of *Hs*HR, also known as HR_{410}, which is not part of the natural photocycle (Hazemoto *et al.*, 1984; Hegemann *et al.*, 1985). Reprotonation of HR_{410} results in a red/violet, anion-free form (Ogurusu *et al.*, 1982) that simulates a potential O-like state. Studies of *Np*HR revealed that structural changes defining the O-like form have already occurred upon the formation of the yellow form and the associated ion release (Kanada *et al.*, 2011; Kouyama *et al.*, 2015).

Recently, we published a new crystal form of *Hs*HR that appeared to be a promising system for the study of light-induced structural changes in the protein as it imposed little restraint on potentially moving regions of the protein through crystal contacts (Schreiner *et al.*, 2015). Here, we present a 2.6 Å resolution structure of *Hs*HR in this crystal form after treatment with basic buffer. The crystal turned yellow and the structure exhibits a depletion in the occupancy of CBS I to about 50%. In contrast to *Np*HR, no significant structural changes within the protein structure could be identified. In this crystal form of *Hs*HR the loss of bound halide ions is apparently not strictly linked to structural changes within the protein backbone.

2. Materials and methods

2.1. Protein production and purification

Protein production and purification of *Hs*HR was performed as described by Schreiner *et al.* (2015). Briefly, *Hs*HR was recombinantly expressed in *H. salinarum* under the control of the strong *bop* promotor. *Hs*HR-containing membrane patches were isolated from lysed cells by several centrifugations in water.

2.2. Protein crystallization and crystal modification

The crystallization procedure of *Hs*HR using the vesicle-fusion method has been described in Schreiner *et al.* (2015). *Hs*HR membrane fragments were adjusted to 50 m*M* Tris pH 8, 100 m*M* NaCl, 0.5% Tween 20 and incubated for 4 h at 25°C and 350 rev min^{-1} or at 4°C overnight. *n*-Octyl-β-D-glucoside (OG) was added to a final concentration of 1–2% and the mixture was incubated for 2 h at 20°C and 350 rev min^{-1}. Solubilized *Hs*HR membrane fragments were concentrated using 50 kDa cutoff Vivaspin concentrators (Sartorius) for 10–15 min at 4000*g* to 4–7 mg ml^{-1} and then directly used in vapour-diffusion experiments. Crystals of unmodified, native *Hs*HR grown in 2.2 *M* ammonium sulfate, 150 m*M* NaCl, 100 m*M* bicine pH 8 (protein concentration 6.6 mg ml^{-1}) were light-adapted under an optical microscope, harvested and cryoprotected in 2.4 *M* ammonium sulfate, 100 m*M* bicine pH 8, 30% trehalose. Cryoprotected crystals were flash-cooled in liquid nitrogen.

To generate the anion-free yellow form, single crystals of *Hs*HR grown in 2.4 *M* ammonium sulfate, 150 m*M* NaCl, 100 m*M* bicine pH 8 (protein concentration 4.9 mg ml^{-1}) were incubated in 2.6 *M* ammonium sulfate pH 10, 100 m*M* glycine pH 10, 25% sucrose for a short time period of $\leq$1–2 min. A change in crystal colour from violet to yellow indicated

formation of the yellow form of *Hs*HR. Treated crystals were flash-cooled in liquid nitrogen. Crystal modification and harvesting was performed under dimmed ambient light.

2.3. Structure determination and refinement

Diffraction data were collected from crystals containing the yellow form of *Hs*HR on beamline X10SA, SLS, Villigen at 100 K and a wavelength of 0.9202 Å using a PILATUS 6M detector. Collection of a 2.6 Å resolution data set from a single native *Hs*HR crystal was performed on ESRF beamline ID23-2 equipped with a MAR Mosaic 225 CCD detector at 100 K and a wavelength of 0.873 Å. All data were indexed and integrated with *XDS* (Kabsch, 2010), scaled with *XSCALE* (Kabsch, 2010) and further analyzed with *AIMLESS* (Evans & Murshudov, 2013) from the *CCP*4 software suite (Winn *et al.*, 2011). For the structure determination of the 2.6 Å resolution native form and the yellow form, the $R_{\rm free}$ flags were copied from the data of isomorphous native *Hs*HR (Schreiner *et al.*, 2015). The structural model of native *Hs*HR (PDB entry 5ahy; Schreiner *et al.*, 2015) was then directly refined against the 2.6 Å resolution data for native *Hs*HR and the yellow form. All refinement procedures were performed in *PHENIX* (Adams *et al.*, 2010). For data-quality control and the assessment of changes within the cofactor conformation and in the position and population of ions and water molecules, only the protein part of the native *Hs*HR model was used in the first rounds of refinement. We started the refinement with several rounds of rigid-body refinement consisting of five macrocycles each. The following refinement steps contained alternating cycles of model building in *Coot* (Emsley *et al.*, 2010) and restrained refinement in *PHENIX*. To reduce model bias, an additional single round consisting of five macrocycles of simulated annealing was performed in the early stages of this alternating procedure.

2.4. Occupancy refinement of chloride in CBS I

The occupancy of the bound halide ion in CBS I was determined and validated as follows in *PHENIX*. Firstly, we refined the occupancy of Cl501 (atom Cl A1263 in PDB entry 5g36) along with coordinates and *B* factors. This resulted in a *B* factor for Cl501 that was too low and thus an apparent underestimation of the occupancy (q = 0.43, B = 33.7 Å^2) as revealed by comparing the relative *B* factor (*i.e.* the *B* factor of Cl501 divided by the mean *B* factor of selected reference atoms from the same structure) of the yellow form with the relative *B* factor of three other *Hs*HR structures in the same crystal form (PDB entries 5ahy and 5ahz and the native 2.6 Å resolution structure reported here). In the calculation of the relative *B* factor we used as references (i) all atoms, (ii) 13 surrounding atoms with a mean distance of 4 Å and a maximum distance of 5.4 Å to the chloride ion and (iii) the side-chain O atom (OG) of Ser115, which is the closest hydrogen-bonded atom. This comparison showed that the relative *B* factor of Cl501 showed the lowest variation between the three structures when Ser115 OG was used as a reference. Therefore, we decided to fix the *B* factor of Cl501 to 1.1 times the value for Ser115 OG. The occupancy of Cl501 was then set to starting values ranging from 0.1 to 0.9. Subsequently, at least two rounds of occupancy refinement consisting of five macrocycles each were carried out until the occupancy converged to stable values (q = 0.54, B = 43.8 Å^2).

To validate the results of the occupancy refinement and to determine the limits for a reasonable occupancy range, we varied the occupancy of the chloride in small steps of 0.05 with respect to the results of the prior occupancy-refinement procedure. The *B* factor was kept constant. In a second step, weighted $F_{\rm o} - F_{\rm c}$ difference density maps were calculated for each individual occupancy value and analyzed for the presence of positive and negative difference density in close vicinity to Cl501. The calculation of electron-density maps was carried out in *PHENIX* (one macrocycle) by switching off all refinement options.

2.5. Structure validation and graphical representation

The fully refined structural models were validated using the *MolProbity* server (Chen *et al.*, 2010) and the validation tools implemented in *Coot*. $F_{\rm o} - F_{\rm c}$ and $2F_{\rm o} - F_{\rm c}$ electron-density maps were calculated with *FFT* from the *PHENIX* software package (Adams *et al.*, 2010) with grid resolution factors of 0.25 and 0.1, respectively. Figures were generated with *PyMOL* (v.1.5.0.3; Schrödinger). *B* factors were normalized as described by Parthasarathy & Murthy (1997) using the equation

$$B_i' = \frac{B_i - \langle B \rangle}{\sigma(B)}, \qquad (1)$$

where B_i is the *B* factor of the *i*th C$^\alpha$ atom in the respective chain, $\langle B \rangle$ is the mean and $\sigma(B)$ is the standard deviation of all *B* factors of the same chain.

2.6. UV–Vis spectroscopy of *Hs*HR membrane patches

A suspension of *Hs*HR-containing membrane patches was diluted in the respective buffer solution to an absorbance of ∼0.3 at 560 nm. The following buffer solutions were used for the pH-dependent measurements: pH 4–7, 100 m*M* trisodium citrate/citric acid, 100 m*M* NaCl; pH 8–9, 100 m*M* bicine, 100 m*M* NaCl; pH 10–11, 100 m*M* glycine, 100 m*M* NaCl. UV–Vis spectra were recorded with a Shimadzu UV2450 two-beam spectrophotometer (Shimadzu Scientific Instruments, Columbia, Maryland, USA) using a 10 mm QS Ultra-Micro cuvette (Type 105.201-QS; Hellma, Müllheim, Germany). The measurements were performed with a medium sampling speed and a sampling rate of 1 nm. To prevent differences in the properties of the cuvettes affecting the overall absorption spectra, the buffer reference was recorded separately against the air background. The same cuvette was used in the following sample measurements and the spectra were also recorded against the air background. For background correction, the buffer reference spectra were subtracted manually from the measured absorption spectra of *Hs*HR.

3. Results and discussion

3.1. Yellow *Hs*HR reveals a poorly occupied CBS I

With the aim of structurally characterizing the ion-transport mechanism of *Hs*HR, we pursued different strategies to trap late-photocycle intermediates in *Hs*HR crystals. Treatment of *Hs*HR with exogenous proton acceptors or basic pH mediates deprotonation of the PSB, which is accompanied by a significant reduction in the binding affinity of CBS I and CBS II (Lanyi & Schobert, 1983; Hegemann *et al.*, 1985; Schobert *et al.*, 1986; Kanada *et al.*, 2011). As trapping of late-photocycle intermediates could not be achieved by photoactivation of *Hs*HR, we transferred *Hs*HR crystals into anion-free basic medium to attain the depletion of the extracellular CBSs, a state that potentially mimics the structural situation in the final stages of *Hs*HR ion transport.

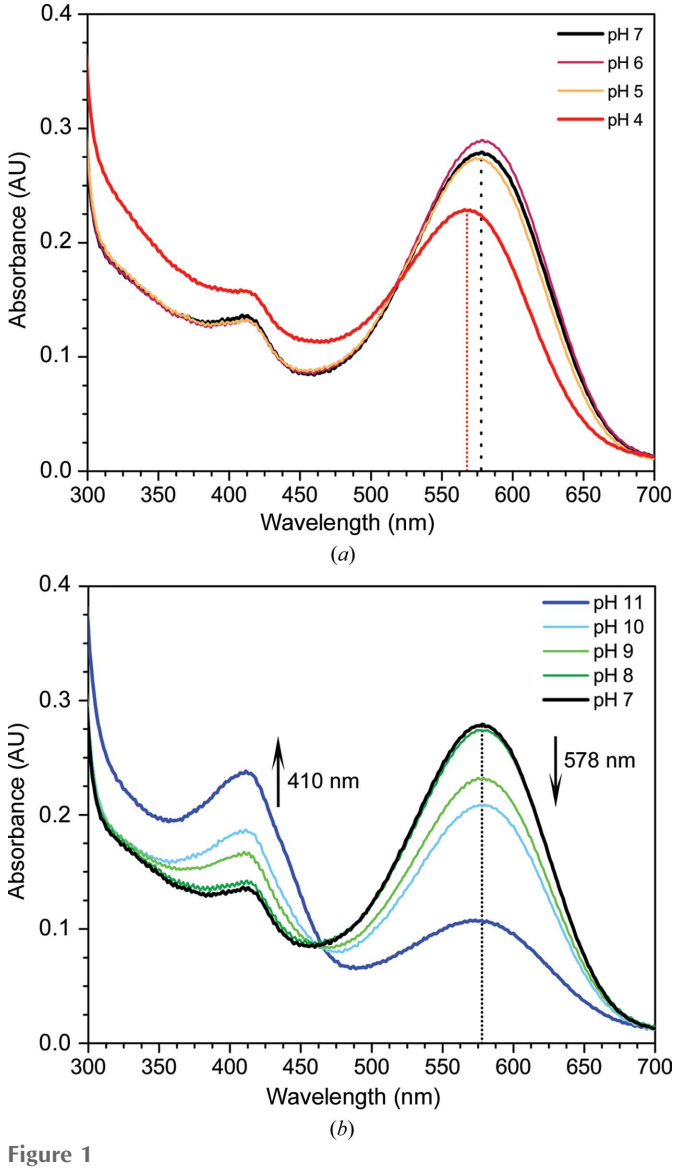

Figure 1
The dependence of *Hs*HR absorbance on variations in pH. The effect of (*a*) acidic or (*b*) basic pH values on *Hs*HR was probed by UV–Vis spectroscopy. (*a*) pH values from 7 to 5 had little effect on the *Hs*HR absorbance. At pH 4 a hypsochromic shift of the maximum at 578 nm to 568 nm was observed. (*b*) An increase in the pH to values of 9 and above led to a decrease in the global maximum at 578 nm accompanied by increased absorbance at 410 nm.

To determine a suitable pH at which *Hs*HR forms a significant proportion of the deprotonated yellow form, we analyzed the effect of variation in pH on the protein by UV–Vis spectroscopy using *Hs*HR-containing membrane patches (Fig. 1). While *Hs*HR absorption was not significantly affected in the range from pH 5 to pH 8, there was a hypsochromic shift of the maximum at 570 nm to 568 nm at pH 4. Similar to observations on bacteriorhodopsin (Mowery *et al.*, 1979), this spectral shift is believed to be induced by the loss of the negative charge in CBS I as a consequence of the loss of the complex counterion (Ogurusu *et al.*, 1982). At basic pH values the absorption at 578 nm decreased, while it increased at 410 nm. We used pH 10 for the generation of the yellow form *in crystallo*. An immediate colour change of the crystal from purple to yellow (Fig. 2*a*) confirmed the successful formation of yellow *Hs*HR.

The structure of the yellow form of *Hs*HR was solved to a resolution of 2.6 Å. For direct comparison, we used a native *Hs*HR structure generated from a data set with similar overall statistics and maximum resolution. The overall data-collection and refinement statistics of both forms are listed in Table 1. There is one molecule in the asymmetric unit. A trimer, as generally observed in HR crystal structures, is generated by crystallographic symmetry. The overall structure of yellow *Hs*HR is essentially identical to the previously published structures in the same crystal form (Schreiner *et al.*, 2015), with an r.m.s.d. for C^{α} atoms of below 0.3 Å.

To identify changes within the retinal chromophore and in the ion and water positions in yellow *Hs*HR as well as in the low-resolution native form, we used only the protein part of the isomorphous high-resolution *Hs*HR structural model (PDB entry 5ahy; Schreiner *et al.*, 2015) in the first rounds of the refinement process. Even the yellow form contained positive $F_o - F_c$ difference density within CBS I at the expected position of the chloride ion and the surrounding water cluster (Fig. 2*b*). Nevertheless, in comparison to native *Hs*HR (Fig. 2*c*) the observable positive $F_o - F_c$ difference density was significantly weaker and $2F_o - F_c$ density was only visible at low contour levels of $\sim 0.7\sigma$ for chloride and ~ 0.8–0.9σ for Wat505b and Wat508 (Fig. 2*d*), indicating an at least partial depopulation of CBS I. In CBS II neither $2F_o - F_c$ density nor positive $F_o - F_c$ density could be detected at the expected position of the chloride ion. This binding site has a low halide-ion affinity and thus can easily be depopulated by a significant decrease in the environmental halide concentration (Falke *et al.*, 1984). As *Hs*HR crystals were grown in a low-chloride condition and were further treated with halide-free post-crystallization and cryoprotection solutions, the chloride of CBS II has most likely been washed out. Thus, it is not surprising that CBS II appears to be vacant in native *Hs*HR as well as the yellow form. We decided to leave this position empty in the final model of yellow *Hs*HR.

To determine the occupancy of the chloride ion bound to CBS I, we performed an occupancy refinement in *PHENIX* (Adams *et al.*, 2010) on the yellow form as described in §2 and,

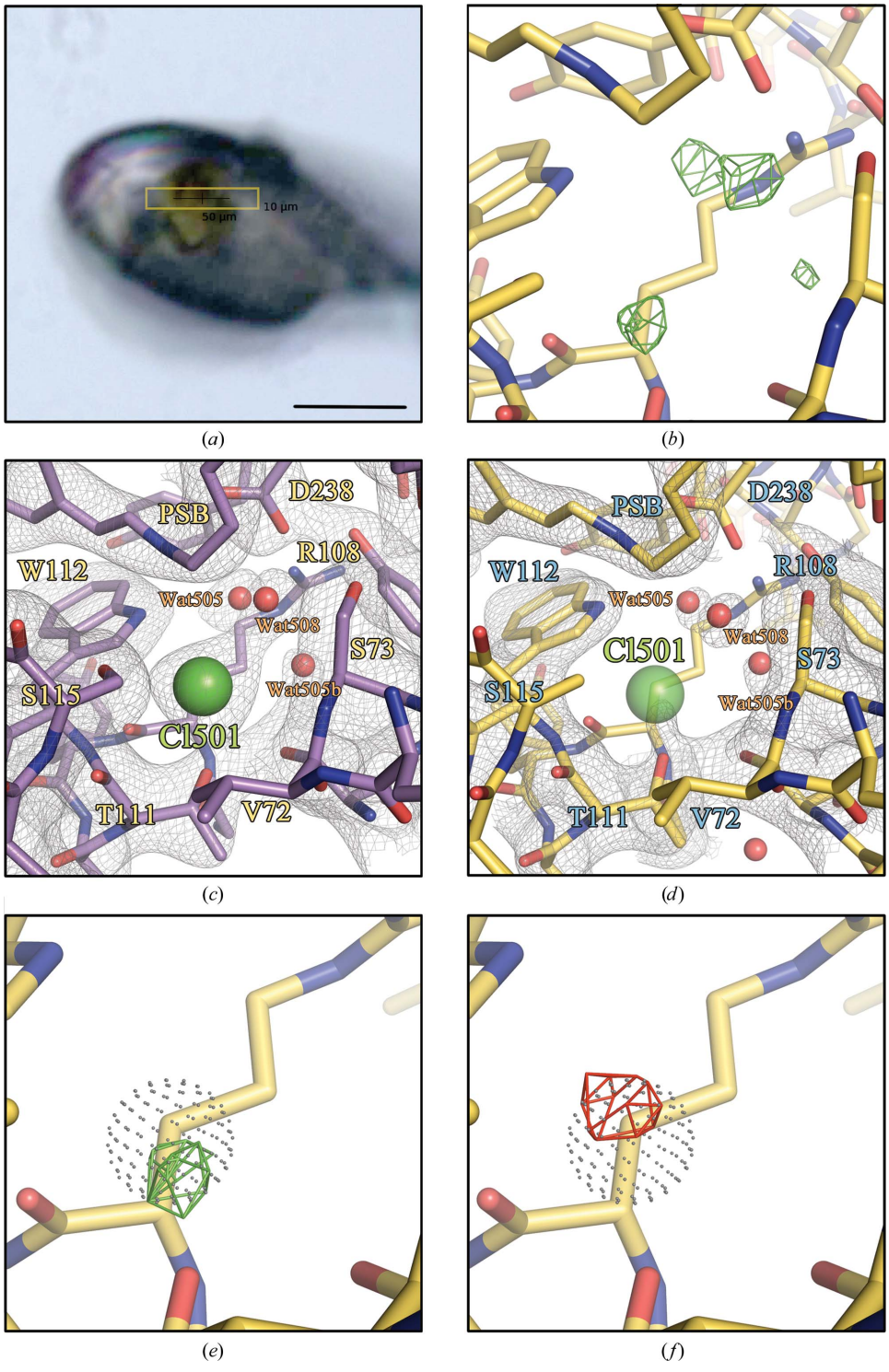

Figure 2
Yellow crystal of *Hs*HR and structure of CBS I. (*a*) Mounted yellow crystal of *Hs*HR used for data collection. The yellow colour of the crystal emphasizes the successful trapping of yellow *Hs*HR *in crystallo*. The picture was taken on beamline X10SA (PXII) at the Swiss Light Source (SLS). The scale bar is 50 µm in length. (*b*) Difference density distribution within CBS I of yellow *Hs*HR after simulated-annealing refinement. The simulated-annealing OMIT $F_o - F_c$ difference density reveals positive peaks at 3.0σ in the cavity of CBS I identical to the chloride ion and water-cluster positions in native *Hs*HR. Green mesh, positive weighted $F_o - F_c$ difference density contoured at 3.0σ. Map calculation was performed in *FFT* with a grid resolution factor of 0.25. (*c*, *d*) Primary chloride-binding sites (CBS I) of native *Hs*HR (ground state) and the yellow form of *Hs*HR. Comparison of CBS I of (*c*) the native, violet form and (*d*) the yellow form of *Hs*HR. $2F_o - F_c$ electron density contoured at 0.9σ is shown as a grey mesh calculated with a grid resolution factor of 0.1. Bound chloride ions and water molecules are illustrated as green and red spheres, respectively. (*e*, *f*) Occupancy assessment of the chloride ion bound in CBS I. To narrow down the range of reasonable occupancy values for Cl501, its occupancy was varied in small steps while keeping the *B* factor fixed. Weighted $F_o - F_c$ difference density maps were calculated in *PHENIX*. For an occupancy of 0.25 positive difference density (*e*) and for an occupancy of 0.75 negative difference density (*f*) appeared at 3.0σ. Cl501 is illustrated as dotted sphere. Green mesh, positive weighted $F_o - F_c$ difference density contoured at 3.0σ; red mesh, negative weighted $F_o - F_c$ difference density contoured at −3.0σ. The grid resolution factor is 0.25.

for direct comparison, also on native *Hs*HR, in which the occupancy was refined during the restrained refinement process. Owing to a considerably higher halide-ion affinity of ∼20 m*M* (Falke *et al.*, 1984; Steiner *et al.*, 1984; Váró, Zimányi *et al.*, 1995) CBS I remains highly occupied even at low halide concentrations, as illustrated by the occupancy value of 1.0 for Cl501 in native *Hs*HR. In contrast, in the yellow form the occupancy of Cl501 (residue A1263 in PDB entry 5g36) converged to ∼0.54 during refinement irrespective of the initial value. The loss of the positive charge owing to deprotonation of the PSB apparently led to depopulation of the CBS I by about 50%. Yet, we could not attain complete depletion of CBS I, as was observed for *Np*HR under similar conditions (Kanada *et al.*, 2011).

3.2. Depletion of CBS I does not cause significant structural changes

As a result of depleting CBS I, the residues Tyr77, Arg108, Thr111, Trp112 and Ser115 that form hydrogen bonds to the chloride ion and the CBS I water cluster under native conditions reoriented to a minimal degree (Figs. 2*c* and 2*d*). Also, the retinal chromophore underwent a slight upwards movement within the region of the now-deprotonated imine bond. Significant structural changes, as had been observed upon formation of the yellow form of *Np*HR (Kanada *et al.*, 2011), could not be identified. Thus, in contrast to *Np*HR, the depletion of CBS I apparently does not necessarily induce conformational changes within the protein backbone in this crystal form of *Hs*HR.

The cavity of CBS I is lined by a distortion, a 3_{10}-helix, within helix C that encompasses Leu110–Ala113. This local variance allows some flexibility within this region. As the 3_{10}-helical region is highly conserved in the HR family, it is considered to be essential for the ion-transport process (Kolbe *et al.*, 2000; Kouyama *et al.*, 2010). A particularly important role has been assigned to Thr111 (Thr126 in *Np*HR). The side chain of Thr111 is inherently flexible as it exists in different rotamers in the ground state of *Hs*HR (Kolbe *et al.*, 2000; Gmelin *et al.*, 2007; Schreiner *et al.*, 2015). In *Np*HR, depletion of CBS I upon formation of the yellow form induces a significant conformational change within the region encompassing Arg123–Ser130 (Arg108–Ser115 in *Hs*HR; Kanada *et al.*, 2011). This process leads to an inward-oriented movement of Thr126 into the site previously occupied by chloride accompanied by a significant shrinkage of the cavity of CBS I. As a nearly identical situation has recently been described for the O-intermediate of *Np*HR (Kouyama *et al.*, 2015), a pivotal role of Thr126 in ion transport to the intracellular ion-export channel has been assumed.

Except for a slight inward rotation of Thr111, we did not observe further structural changes within the 3_{10}-helix in the yellow form of *Hs*HR. Nevertheless, the movement of helix C should not be restricted by the crystal lattice, as helix C faces inwards in all monomers of the *Hs*HR trimer. This situation is identical to *Np*HR, and helix C is not involved in contacts between HR trimers in our crystals of *Hs*HR. A comparison of the normalized *B* factors (Fig. 3) of the low- and high-resolution structural models of native *Hs*HR (this study and PDB entry 5ahy, respectively), the bromide-bound variant (PDB entry 5ahz) and the yellow form reveals higher flexibility of the latter in the region encompassing Arg108–Ser115. The local maximum around Tyr109–Thr111, the section believed to be essential for ion transport, might indicate the beginning of a conformational change that might have been trapped before completion of the whole process. In the yellow form, the connection between helices E and F and the N-terminal part of helix F (around residues 190–200) also show a pronounced increase in *B* factor compared with the low-resolution native form (Fig. 3*a*), which is less striking when compared with the published structures with PDB codes 5ahy and 5ahz (Fig. 3*b*). It is interesting to note that the equivalent region in *Np*HR undergoes light-induced confor-

Table 1
X-ray data-collection and refinement statistics for halorhodopsin.

Values in parentheses are for the highest resolution shell.

Data set	Native	Yellow form
Data collection		
Diffraction source	ID23-2, ESRF	X10SA, SLS
Wavelength (Å)	0.8726	0.9202
Temperature (K)	100	100
Detector	MAR Mosaic 225 CCD	PILATUS 6M
Detector distance (mm)	306.4	555.0
Rotation per image (°)	1	0.1
Total rotation (°)	164	130
Exposure time (s)	1.0	0.098
Space group	*R*32	*R*32
Unit-cell parameters (Å, °)	$a = b = 103.5$, $c = 137.8$, $\alpha = \beta = 90$, $\gamma = 120$	$a = b = 103.0$, $c = 136.5$, $\alpha = \beta = 90$, $\gamma = 120$
Mosaicity (°)	0.171	0.287
Resolution range (Å)	42.6–2.6 (2.73–2.60)	45.5–2.6 (2.73–2.60)
No. of observed reflections	90850	71619
No. of unique reflections	8947	8774
Completeness (%)	100 (100)	99.91 (99.77)
Multiplicity	10.2 (10.3)	8.2 (5.7)
$R_{\rm p.i.m.}$† (%)	9.3 (47.1)	6.2 (41.0)
Mean $I/\sigma(I)$	12.8 (1.8)	14.5 (1.8)
$CC_{1/2}$	0.998 (0.702)	0.998 (0.637)
Wilson *B* factor (Å^2)	34.5	34.1
Refinement		
$R_{\rm work}/R_{\rm free}$‡ (%)	19.4 (22.4)/25.2 (29.7)	19.1 (21.9)/25.3 (32.1)
Mean *B* factor (Å^2)		
Overall	43.2	36.6
Protein	43.1	36.1
Ligand/ion	51.1	45.6
Water	33.5	32.6
No. of atoms		
Protein	1842	1862
Ligand/ion	21	21
Water	11	13
R.m.s.d.		
Bond lengths (Å)	0.009	0.007
Angles (°)	0.995	1.00
Ramachandran plot		
Favoured (%)	98.4	98.0
Allowed (%)	1.6	2.0

† $R_{\rm p.i.m.} = \sum_{hkl}\{1/[N(hkl)-1]\}^{1/2}\sum_i |I_i(hkl) - \langle I(hkl)\rangle|/\sum_{hkl}\sum_i I_i(hkl)$, where $I_i(hkl)$ is the *i*th measurement and $N(hkl)$ is the redundancy of reflection *hkl*. ‡ $R_{\rm work} = \sum_{hkl}||F_{\rm obs}| - |F_{\rm calc}||/\sum_{hkl}|F_{\rm obs}|$. $R_{\rm work}$ was calculated from the work set. $R_{\rm free}$ was calculated from a test set encompassing 5% of the total reflections. The test set was not used in refinement.

mational changes (Nakanishi *et al.*, 2013). In *Np*HR the formation of the yellow form is accompanied by an overall significant alteration of the unit-cell axis lengths and a change in the arrangement of the protein (Kanada *et al.*, 2011). When we incubated *Hs*HR crystals in basic buffer for significantly longer periods we observed a complete loss of diffraction. It is conceivable that upon prolonged incubation in basic buffer *Hs*HR indeed underwent structural changes that, in contrast to *Np*HR, destroyed the crystalline order.

In conclusion, we could not detect significant structural changes upon the formation of yellow *Hs*HR and the associated ion release. These results indicate that in this crystal form of *Hs*HR the depopulation of CBS I is not directly linked to movements within the protein, as these may be hindered by crystal-packing contacts. Nevertheless, as the 3_{10}-helical region of helix C reveals an increased flexibility in our structural model of yellow *Hs*HR, this section presumably plays a pivotal role in protein function. Similar to *Np*HR, the 3_{10}-helical region might indeed be obligatory in order to regulate and warrant unidirectional ion transport.

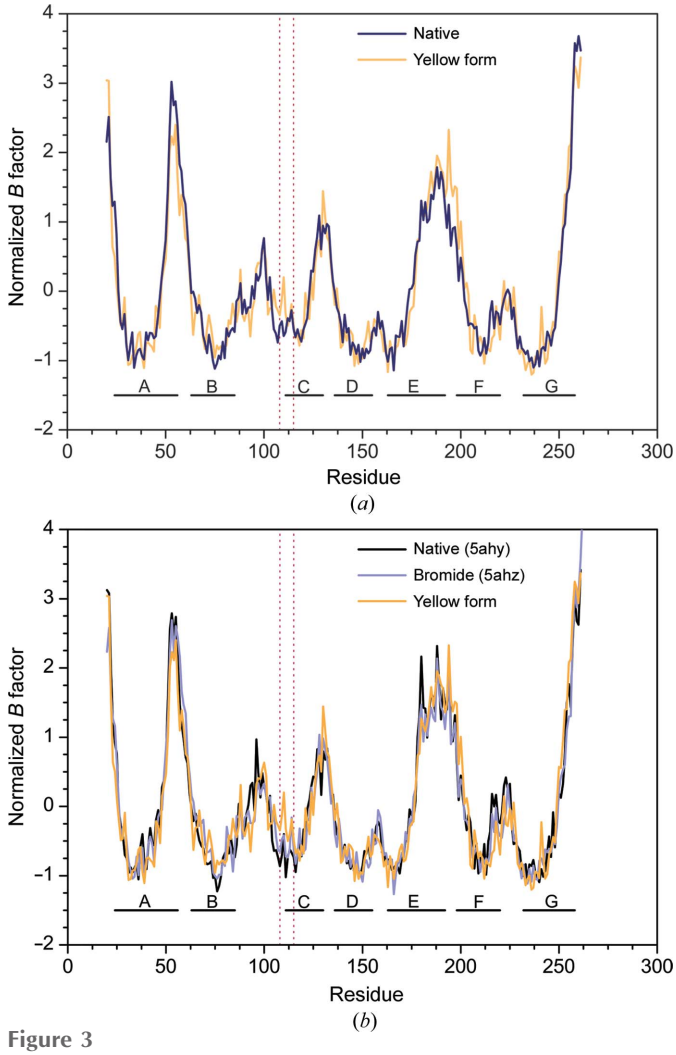

Figure 3
Normalized *B*-factor plots. (*a*) Comparison of the yellow form and native *Hs*HR at 2.6 Å resolution. (*b*) Comparison of the yellow form with native *Hs*HR at 2.2 Å resolution (PDB entry 5ahy) and the bromide-bound form (PDB entry 5ahz). Residues that have been described to undergo a significant structural change in *Np*HR upon formation of the yellow form are framed by red dotted lines.

Acknowledgements

This project was funded by grants from the Deutsche Forschungsgemeinschaft (Collaborative Research Centre 613, Project D11 to JH and HHN, and the FOR-1279 'Protein-based photoswitches as optogenetic tools' to RS and JH). Dorothea Heinrich (FU Berlin) and Ramona Justinger (Research Center Jülich) are acknowledged for excellent technical assistance in preparing large quantities of purified *Hs*HR. Diffraction experiments were performed on the ID23-2 beamline at the European Synchrotron Radiation Facility (ESRF), Grenoble, France and beamline X10SA (PXII) at the Swiss Light Source (SLS), Villigen, Switzerland. We are grateful to Antoine Royant at ESRF and Florian Dworkowski at SLS for providing assistance in using beamlines ID23-2 and X10SA (PXII), respectively. We acknowledge financial support for travel to the ESRF through BAG MX-1284. We thank Heide Marie Roth and Marcus Resch (University of Göttingen) for collection of the native data set.

References

Adams, P. D. *et al.* (2010). *Acta Cryst.* D**66**, 213–221.
Ames, J. B., Raap, J., Lugtenburg, J. & Mathies, R. A. (1992). *Biochemistry*, **31**, 12546–12554.
Chen, V. B., Arendall, W. B., Headd, J. J., Keedy, D. A., Immormino, R. M., Kapral, G. J., Murray, L. W., Richardson, J. S. & Richardson, D. C. (2010). *Acta Cryst.* D**66**, 12–21.
Emsley, P., Lohkamp, B., Scott, W. G. & Cowtan, K. (2010). *Acta Cryst.* D**66**, 486–501.
Evans, P. R. & Murshudov, G. N. (2013). *Acta Cryst.* D**69**, 1204–1214.
Falb, M., Müller, K., Königsmaier, L., Oberwinkler, T., Horn, P., von Gronau, S., Gonzalez, O., Pfeiffer, F., Bornberg-Bauer, E. & Oesterhelt, D. (2008). *Extremophiles*, **12**, 177–196.
Falke, J. J., Chan, S. I., Steiner, M., Oesterhelt, D., Towner, P. & Lanyi, J. K. (1984). *J. Biol. Chem.* **259**, 2185–2189.
Gmelin, W., Zeth, K., Efremov, R., Heberle, J., Tittor, J. & Oesterhelt, D. (2007). *Photochem. Photobiol.* **83**, 369–377.
Guijarro, J., Engelhard, M. & Siebert, F. (2006). *Biochemistry*, **45**, 11578–11588.
Hazemoto, N., Kamo, N. & Kobatake, Y. (1984). *Biochem. Biophys. Res. Commun.* **118**, 502–507.
Hegemann, P., Oesterhelt, D. & Steiner, M. (1985). *EMBO J.* **4**, 2347–2350.
Kabsch, W. (2010). *Acta Cryst.* D**66**, 125–132.
Kanada, S., Takeguchi, Y., Murakami, M., Ihara, K. & Kouyama, T. (2011). *J. Mol. Biol.* **413**, 162–176.
Kolbe, M., Besir, H., Essen, L.-O. & Oesterhelt, D. (2000). *Science*, **288**, 1390–1396.
Kouyama, T., Kanada, S., Takeguchi, Y., Narusawa, A., Murakami, M. & Ihara, K. (2010). *J. Mol. Biol.* **396**, 564–579.
Kouyama, T., Kawaguchi, H., Nakanishi, T., Kubo, H. & Murakami, M. (2015). *Biophys. J.* **108**, 2680–2690.
Lanyi, J. K. (1990). *Physiol. Rev.* **70**, 319–330.
Lanyi, J. K. & Schobert, B. (1983). *Biochemistry*, **22**, 2763–2769.
Luisi, B. F., Lanyi, J. K. & Weber, H. J. (1980). *FEBS Lett.* **117**, 354–358.
Mowery, P. C., Lozier, R. H., Chae, Q., Tseng, Y.-W., Taylor, M. & Stoeckenius, W. (1979). *Biochemistry*, **18**, 4100–4107.
Mukohata, Y. & Kaji, Y. (1981). *Arch. Biochem. Biophys.* **206**, 72–76.

Nakanishi, T., Kanada, S., Murakami, M., Ihara, K. & Kouyama, T. (2013). *Biophys. J.* **104**, 377–385.
Ogurusu, T., Maeda, A., Sasaki, N. & Yoshizawa, T. (1982). *Biochim. Biophys. Acta*, **682**, 446–451.
Parthasarathy, S. & Murthy, M. R. N. (1997). *Protein Sci.* **6**, 2561–2567.
Reed, C. J., Lewis, H., Trejo, E., Winston, V. & Evilia, C. (2013). *Archaea*, **2013**, 373275.
Rüdiger, M. & Oesterhelt, D. (1997). *EMBO J.* **16**, 3813–3821.
Schobert, B. & Lanyi, J. K. (1982). *J. Biol. Chem.* **257**, 10306–10313.
Schobert, B., Lanyi, J. K. & Oesterhelt, D. (1986). *Biol. Chem.* **261**, 2690–2696.
Schreiner, M., Schlesinger, R., Heberle, J. & Niemann, H. H. (2015). *J. Struct. Biol.* **190**, 373–378.
Spencer, D. B. & Dewey, T. G. (1990). *Biochemistry*, **29**, 3140–3145.
Steiner, M., Oesterhelt, D., Ariki, M. & Lanyi, J. K. (1984). *J. Biol. Chem.* **259**, 2179–2184.
Váró, G., Brown, L. S., Sasaki, J., Kandori, H., Maeda, A., Needleman, R. & Lanyi, J. K. (1995). *Biochemistry*, **34**, 14490–14499.
Váró, G., Needleman, R. & Lanyi, J. K. (1995). *Biochemistry*, **34**, 14500–14507.
Váró, G., Zimányi, L., Fan, X., Sun, L., Needleman, R. & Lanyi, J. K. (1995). *Biophys. J.* **68**, 2062–2072.
Winn, M. D. *et al.* (2011). *Acta Cryst.* D**67**, 235–242.
Zimányi, L. & Lanyi, J. K. (1989). *Ann. N. Y. Acad. Sci.* **574**, 11–19.